Applied Physics A (2024) 130:25
https://doi.org/10.1007/s00339-023-07172-1

**Applied Physics A**
**Materials Science & Processing**

# Red/deep-red emitting phosphors of $Eu^{3+}/Dy^{3+}$ co-doped $NaSrGd(WO_4)_3$ for LED and optical anti-counterfeiting

**Hong Liu[1] · Wanhang Li[1] · Huihua Ye[1] · Rui Hu[1] · Jinfeng Lin[1] · Shiyin Tan[1] · Xusheng Wang[1] · Yanxia Li[1] · Xi Yao[1]**

Received: 28 September 2023 / Accepted: 15 November 2023 / Published online: 14 December 2023


**Abstract**
The family of rare-earth doped phosphors has drawn pronounced attention in technological of fingerprint visualization, anti-counterfeiting, and phosphor-converted light-emitting diodes applications. A series of $NaSrGd_{(1-x-y)}Eu_xDy_y(WO_4)_3$ powder luminescent materials were synthesized by a solid-state reaction. The emission color of $NaSrGd(WO_4)_3$:$Dy^{3+}$ phosphor could be tunned via changing concentrations of $Eu^{3+}$ ion. In addition, the phosphors exhibit narrow red-light emission at 610 nm caused by the electric dipole transition $^5D_0 \rightarrow {}^7F_2$ of $Eu^{3+}$. Especially, the phosphor exhibits superior thermal stability, its emission intensity of optimum sample remained ± 15% over the temperature range from 233 to 393 K. The Commission International de I'Eclairage (CIE) chromaticity coordinates of $x = 0.4$ are (0.6388, 0.3371) with a high color purity (92.84%). More importantly, prepared color-changing device of phosphors achieves a high level of optical safety. The results demonstrate that their materials can be potentially applied to the field of white light-emitting diodes (LEDs) and optical anti-counterfeiting.

**Keywords** Phosphors · Rare-earth doped · Anti-counterfeiting · $Eu^{3+}$ ion · Solid-state reaction

## 1 Introduction

LEDs with excellent luminous performance and environmentally friendly characteristics possess a broad range of application prospects in diverse fields, for example, urban renewal, rural ecological enhancement, intelligent manufacturing, smart lighting, safety production, and emergency management [1–5]. Significant research efforts are being focused on enhancing various aspects of LED devices for the development of next-generation white LEDs, which include improving color rendering performance, luminous intensity, service life, and thermal stability while maintaining cost-effectiveness [3–5].

In the realm of white-LED applications, blue and green phosphors have reached a more advanced stage compared to red phosphors [6–9]. The latter, with their higher luminous efficiency, superior color temperature, and color rendering performance, still require significant exploration and improvement. The extensive use of white LEDs with tricolor phosphors, particularly those excited by near-ultraviolet light, necessitates the research and development of red phosphors with enhanced luminescence properties. An optimal red phosphor should efficiently capture light energy in the near-ultraviolet region and emit pure red light. Additionally, it should be made from inexpensive raw materials, have an appropriate sintering temperature, and exhibit excellent thermal stability [7, 8]. In particular, the large-scale deployment of white LEDs with tricolor phosphors, especially those excited by near-ultraviolet light, underscores the urgency to study and develop red phosphors with better luminescence performance. These red phosphors should exhibit a strong ability to capture light energy in the near-ultraviolet region and emit pure red light. Moreover, they should also utilize affordable raw materials, possess a suitable sintering temperature, and display good thermal stability [6–9].

The rare-earth $Eu^{3+}$ ions, with their characteristic emission peak at ~ 610 nm due to the $^5D_0 \rightarrow {}^7F_2$ transition, exhibit red light [10–15]. Their good chemical stability and excellent luminescence performance make them ideal as luminescent centers for white LED red phosphors [2, 13]. On the other hand, the tungstate compound, with its $(WO_4)^{2-}$ group, can effectively absorb blue-violet light [11, 16–19]. It also exhibits a strong and wide charge transfer band (CTB) in the near-ultraviolet region around 200–300 nm, indicating

✉ Xusheng Wang
xs-wang@tongji.edu.cn

[1] Functional Materials Research Laboratory, School of Materials Science and Engineering, Tongji University, Shanghai 201804, China

high absorption and transfer efficiency to near-ultraviolet (NUV) excitation light, which benefits the luminous intensity of fluorescent materials. Therefore, the advantages of structural stability and eco-friendliness make tungstate a suitable matrix material for matching near-ultraviolet light chips. When $Eu^{3+}$ ions are combined with a tungstate matrix, the resulting doped materials can enhance the efficiency of the $^5D_0 \rightarrow {}^7F_2$ transitions of the $Eu^{3+}$ ions, resulting in a dominant red light with high color purity [11, 19].

Along this way, a series of $NaSrGd_{(1-x-y)}Eu_xDy_y(WO_4)_3$ powder luminescent materials were synthesized by a solid-state reaction [20, 21]. The emission color of $NaSrGd(WO_4)_3$:$Dy^{3+}$ phosphor could be tunned via changing concentrations of $Eu^{3+}$ ion. In addition, the phosphors exhibit narrow red-light emission at 610 nm caused by the electric dipole transition $^5D_0 \rightarrow {}^7F_2$ of $Eu^{3+}$. Especially, the phosphor exhibits superior thermal stability, its emission intensity of optimum sample remained ± 15% over the temperature range from 233 to 393 K. The Commission International de I'Eclairage (CIE) chromaticity coordinates of $x = 0.4$ are (0.6388, 0.3371) with a high color purity (92.84%). More importantly, prepared color-changing device of phosphors achieves a high level of optical safety. Therefore, the $Eu^{3+}$-activated $NaSrGd(WO_4)_3$ phosphor is a promising material for white light-emitting diodes (LEDs) and optical anti-counterfeiting applications.

## 2 Experimental

### 2.1 Synthesis of $NaSrGd_{(1-x-y)}Eu_xDy_y(WO_4)_3$ series samples

Phosphor samples were synthesize in solid-phase reaction method according to the stoichiometric ratio of $NaSrGd_{(1-x-y)}Eu_xDy_y(WO_4)_3$ ($x = 0.0$, 0.05, 010, 0.15, 0.20, 0.25, 0.30, 0.35, 0.40; $y = 0.05$). The mixture of sodium carbonate ($NaCO_3$, AR 99.8%), strontium carbonate ($SrCO_3$, AR 99%), tungsten oxide ($WO_3$, AR 99%), dysprosium oxide ($Dy_2O_3$, 99.9%), gadolinium oxide ($Gd_2O_3$, 99.95%), and europium oxide ($Eu_2O_3$, 99.99%) was ground in an agate mortar, then placed in air and pre-fired at 600 °C. After sintered at 800–1200 °C in air for 4 h, the series phosphor samples were obtained by grinding again.

### 2.2 Characterization

Thermogravimetric analysis of the test samples was carried out by a STA 449 C thermal analyzer manufactured by NETZSCH, Germany. X-ray diffraction (XRD, HaoYuan Co. Ltd.) and scanning electron microscopy coupled with energy-dispersive X-ray (EDX) spectroscopy (SEM, FEI Quanta200 FEG) were used to characterize the phase structures, as well as the particle size and composition of the samples. Static fluorescence excitation and emission spectra at room/high temperature were recorded with an F-7000 fluorescence spectrometer (Hitachi) equipped with specimen heating holder (THMS 600, Linkam).

## 3 Results and discussion

In order to explore the sintering temperature range of the samples, the raw powder mixture $NaSrGd_{(1-x-y)}Eu_xDy_y(WO_4)_3$ ($x = 0.20$, $y = 0.05$) was measured using TG–DTA, as presented in Fig. 1. The first weight loss step is about 2% from room temperature to about 110 °C, which is mainly ascribed to the evaporation of the adsorbed water, crystal water and ethanol solvent. When the temperature from 110 to 800 °C, the weight loss originates from decomposition of carbonate and the melting of oxide. When the temperature over 800 °C, the reaction of $NaSrGd_{(1-x-y)}Eu_xDy_y(WO_4)_3$ ($x = 0.20$, $y = 0.05$) is completed, indicative of crystallized. Therefore, the $NaSrGd_{(1-x-y)}Eu_xDy_y(WO_4)_3$ ($x = 0.20$, $y = 0.05$) phosphor can be calcined at 800–1200 °C for 4 h to obtain full grain growth and uniform dispersion.

$NaSrGd_{(1-x-y)}Eu_xDy_y(WO_4)_3$ ($x = 0.20$, $y = 0.05$) phosphor samples are prepared with different annealed at 800–1200 °C for 4 h. Figure 2a shows the XRD patterns of $NaSrGd_{(1-x-y)}Eu_xDy_y(WO_4)_3$ ( $x = 0.20$, $y = 0.05$) phosphor sintered at 800 °C, 900 °C, 1000 °C, 1100 °C, and 1200 °C, respectively. The diffraction peaks of all the samples exactly agree with the standard PDF#51-1855 in the JCPDS card, indicating formed a pure phase with tetragonal scheelite structure (I41/a(88) space group ($a = b = 5.3$ Å, $c = 11.5$ Å, $\alpha = \beta = \gamma = 90°$, $V = 323.0$ Å$^3$)) [22]. The $Eu^{3+}$ ($r = 0.947$ Å, CN = 6), $Dy^{3+}$ ($r = 0.912$ Å, CN = 6) and $Gd^{3+}$ ($r = 0.938$ Å, CN = 6) are of similar radii and chemical properties, thus

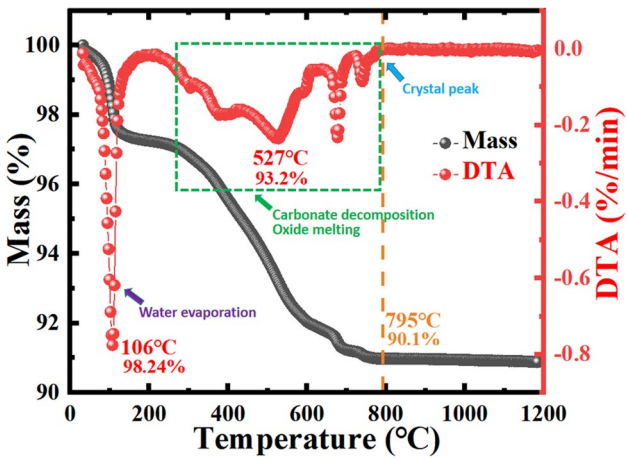


**Fig. 1** TG-DAT spectra of $NaSrGd_{(1-x-y)}Eu_xDy_y(WO_4)_3$ ($x = 0.20$, $y = 0.05$) phosphor samples

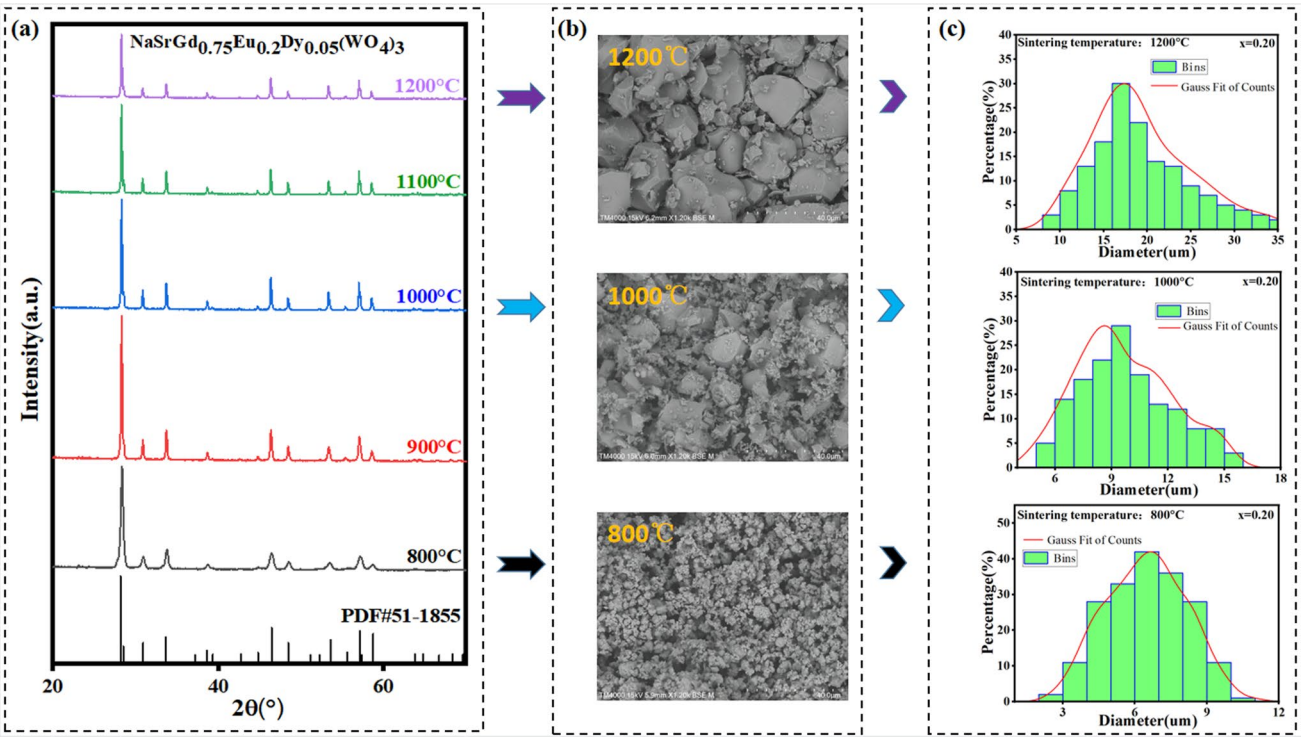


**Fig. 2** **a** XRD of $NaSrGd_{0.75}Eu_{0.2}Dy_{0.05}(WO_4)_3$ phosphor sintered at 800–1200 °C. **b** SEM images of $NaSrGd_{0.75}Eu_{0.2}Dy_{0.05}(WO_4)_3$ samples at sintering temperatures of 800 °C, 1000 °C and 1200 °C at a magnification of 1200 times. **c** Particle size distribution diagram and Gaussian fitting image of $NaSrGd_{0.75}Eu_{0.2}Dy_{0.05}(WO_4)_3$ samples sintered at 800 °C, 1000 °C and 1200 °C

$Eu^{3+}$ions and $Dy^{3+}$ions are most likely to replace $Gd^{3+}$ sites forming $NaSrGd_{0.90}Eu_{0.05}Dy_{0.05}(WO_4)_3$ crystal. With the calcination temperature increasing from 800 to 1200 °C, the XRD diffraction peaks become narrower, indicative crystallinity of it increases significantly [23]. The SEM images of the samples sintered at 800 °C, 1000 °C and 1200 °C are presented in Fig. 2b. Obviously, the grain sizes of $NaSrGd_{(1-x-y)}Eu_xDy_y(WO_4)_3$ ($x=0.20$, $y=0.05$) samples significantly increases as the annealing temperature changes, e.g. ~ 7.5 μm at 800 °C, ~ 11.2 μm at 1000 °C, and ~ 17.5 μm at 1200 °C (Fig. 2c), which is basically consistent with the XRD pattern characteristics.

XRD measurements conducted on the $NaSrGd_{(1-x)}Eu_xDy_{0.05}(WO_4)_3$ ($x=0.10$, 0.15, 0.20, 0.25, 0.30) co-doped phosphors sintered at 1200 °C are displayed in Fig. 3a. Clearly, the positions peaks of all the compositions are well assigned to the standard diffraction pattern (JCPDS- PDF#51-1855), implying that a pristine crystal phase is acquired for the synthesized phosphors. The enlarged diffraction peak ~ 28.3° is shown in Fig. 3c. As the $Eu^{3+}$-doping concentration increases ($x \leq 0.25$), the diffraction peak shifts slightly to lower angle, owing to the substitution of $Gd^{3+}$ ($r=0.94$ Å) by larger $Eu^{3+}$ ($r=1.07$ Å) ions. When $x > 0.25$, the diffraction peak moves slightly to larger angle due to $Sr^{2+}$ site substituted by the interstitial $Eu^{3+}$ codopants [24, 25]. The crystal structure of $NaSrGd_{(1-x)}Eu_xDy_{0.05}(WO_4)_3$ is displayed in Fig. 3d, proving the unit cell belongs to tetragonal scheelite structure. The morphology of the $NaSrGd_{(1-x)}Eu_xDy_{0.05}(WO_4)_3$ co-doped phosphors is studied through SEM, as illustrated in Fig. 3b. The irregular polyhedron shape and relatively uniform grain distribution of $NaSrGd_{(1-x)}Eu_xDy_{0.05}(WO_4)_3$ phosphors are obtained, indicative their high-quality.

The 4f-4f electron transitions of $Eu^{3+}$ ions are highly responsive to changes in the crystal field environment, resulting in a change in the emission peak shape as the matrix material change. Noted that the peak positions and numbers of the characteristic emission peaks of $Eu^{3+}$ ions in the fluorescence spectrum are generally unaffected by a longer fluorescence lifetime compared to $Eu^{2+}$ ions. Figure 4 shows the normalized excitation spectra of $NaSrGd_{(1-x)}Eu_xDy_{0.05}(WO_4)_3$ ($x=0.05$, 0.10, 0.15, 0.20, 0.25, 0.30, 0.35, 0.40) samples. The excitation spectra monitored at 616 nm (Fig. 4a), narrow excitation peaks from 350 to 500 nm can also be observed from the excitation spectra, which could be attributed to the 4f-4f transitions of $Eu^{3+}$ ions. The peaks at 393 nm and 464 nm are attributed to the $^7F_0 \rightarrow {}^5L_6$ and $^7F_0 \rightarrow {}^5D_2$ transition of $Eu^{3+}$ ions. When the $Eu^{3+}$-doping concentration is below 25%, the emission peak in both the NUV and blue regions increases with an

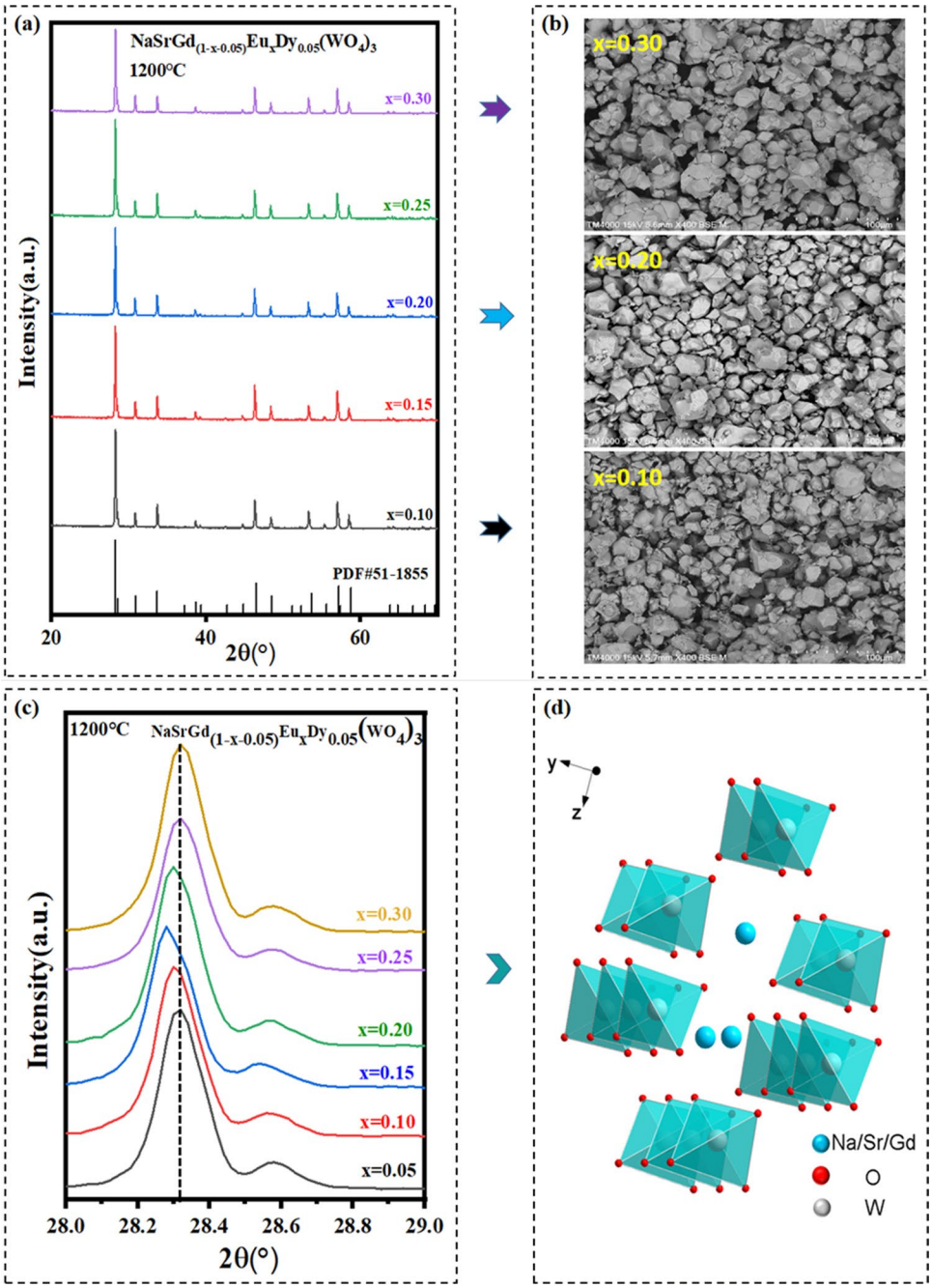


**Fig. 3** **a** XRD Diagram of $NaSrGd_{(1-x-y)}Eu_xDy_y(WO_4)_3$ fluorescent powder; **b** SEM diagram of $NaSrGd_{(1-x-y)}Eu_xDy_y(WO_4)_3$ samples at 400 times magnification; **c** The XRD main peak amplification of $NaSrGd_{(1-x-y)}Eu_xDy_y(WO_4)_3$ samples; **d** Crystal structure of $NaSrGd_{(1-x-y)}Eu_xDy_y(WO_4)_3$ samples

increase in $Eu^{3+}$ ion concentrations. The excitation intensity reaches its maximum value at 25%. However, beyond this point, the intensity of excitation peaks decreases due to the phenomenon of concentration quenching.The process of concentration quenching for $Eu^{3+}$ ions in the matrix material can be summarized as follows: initially, as the concentration of $Eu^{3+}$ ions increases, the number of luminescent centers grows, leading to an increase in luminescent intensity. This continues until the doping concentration reaches its critical concentration-quenching value, at which point the distance between $Eu^{3+}$ ions becomes critical. As a result, the likelihood of energy transfer between the luminescent centers increases, while non-radiative relaxation among the quenching centers leads to more energy quenching processes.

The excitation spectra monitored at 393 nm (Fig. 4b), the strongest emission peak at 616 nm could be observed. A strong emission peak at 610 nm can be attributed to the $^5D_0 \rightarrow {}^7F_2$ characteristic transitions of $Eu^{3+}$ ions [24–27]. Another noticeable emission peak appears at 588 nm, originating from the $^5D_0 \rightarrow {}^7F_1$ characteristic transitions of $Eu^{3+}$ ions. Noted that the $^5D_0 \rightarrow {}^7F_1$ transition is an electric dipole

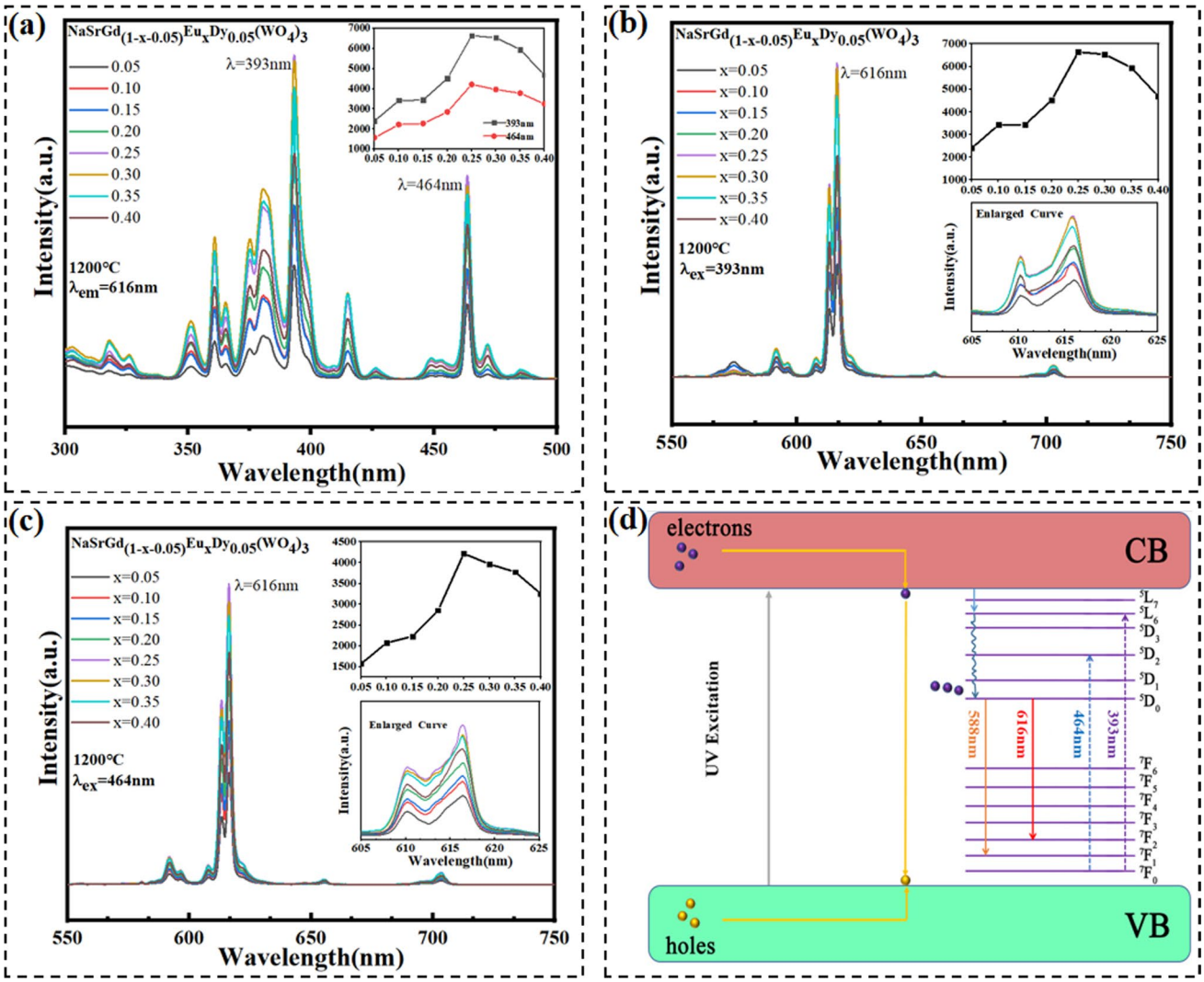


**Fig. 4** **a** Excitation spectra of the $NaSrGd_{(1-x-0.05)}Eu_xDy_{0.05}(WO_4)_3$ phosphors ($\lambda_{em}$ = 616 nm); **b** Emission spectra of the $NaSrGd_{(1-x-0.05)}Eu_xDy_{0.05}(WO_4)_3$ samples ($\lambda_{ex}$ = 393 nm); **c** Emission spectra of the $NaSrGd_{(1-x-0.05)}Eu_xDy_{0.05}(WO_4)_3$ samples ($\lambda_{ex}$ = 464 nm); **d** Schematic diagram of energy level transition of the $NaSrGd_{(1-x-0.05)}Eu_xDy_{0.05}(WO_4)_3$ sample

transition, while the $^5D_0 \rightarrow {}^7F_2$ transition is a magnetic dipole transition. The observation of a stronger intensity in the $^5D_0 \rightarrow {}^7F_2$ transition compared to the $^5D_0 \rightarrow {}^7F_1$ transition suggests that the $Eu^{3+}$ ions occupy asymmetric crystal sites [26, 27]. The fluorescence spectrum confirms this finding. Due to the splitting of the emission peak resulting from the $^5D_0 \rightarrow {}^7F_2$ transition, two peaks with similar intensities are formed. This further supports the presence of $Eu^{3+}$ ions in an asymmetric local crystal environment. The distortion of the crystal lattice symmetry enhances the splitting degree of the $^7F_2$ energy level, contributing to the appearance of multiple split emission peaks at 610 nm and 616 nm in the fluorescence spectrum. Compared with other $Eu^{3+}$-activated luminophor, the emission peak position of samples shows no obvious transformation, the emission spectrum of the excitation spectra monitored at 393 nm is well agreement with excitation spectra monitored at 464 nm [24–27]. And their emission intensity is relatively weak, indicating a low excitation efficiency in the blue region. According to the above analysis, this phosphor sample is more matched with the near ultraviolet chip as compared with blue chip [28].

The luminescence mechanism of $NaSrGd_{(1-x)}Eu_xDy_{0.05}(WO_4)_3$ samples is further investigated, as demonstrated in Fig. 4d. The presence of $Eu^{3+}$ ions as the main luminescent centers in the $NaSrGd(WO_4)_3$ matrix is confirmed. Under excitation by 393 nm ultraviolet light, electrons in the ground state of $Eu^{3+}$ undergo a transfer to the $^5L_6$ level, followed by a jump to the $^5D_0$ level through a non-radiative relaxation process. Finally, they return to the ground state via radiative transitions, resulting in down-conversion luminescence. Additionally, under the excitation of ultraviolet light, the separation of electron–hole pairs occurs,

with some of these pairs entering the conduction band and recombining with the $Eu^{3+}$ luminescent centers, leading to the emission of fluorescent light [29–32].

The band gap of $NaSrGd_{(1-x-y)}Eu_xDy_y(WO_4)_3$ sample can be estimated by according to the following formula:

$$\left[F(R_\infty)h\nu\right]^n = A(h\nu - E_g), \tag{1.1}$$

where $F(R_\infty)$ is Kubelka–Munk function, because the $NaSrGd(WO_4)_3$ matrix absorption is a direct absorption, so $n=2$. A is the scale constant, and $h\nu$ is the energy of each photon. The Kubelka–Munk function $F(R_\infty)$ can be expressed as:

$$F(R_\infty) = \frac{(1-R)^2}{2R} = K/S, \tag{1.2}$$

where $R$ is the reflection coefficient, $K$ is the absorption coefficient, and S is the scattering parameter. The relation curve $\left[F(R_\infty)h\nu\right]^2$ with $h\nu$ is drawn according to Taus method.The optical band gap diagrams of $NaSrGd_{(1-x-y)}Eu_xDy_y(WO_4)_3$ samples are shown in Fig. 5a and b. The $E_g$ of the $NaSrGd(WO_4)_3$ sample is 3.73 eV. In general, the introduction of $Eu^{3+}$ and $Dy^{3+}$ ions significantly reduces the band gap of $NaSrGd_{(1-x-y)}Eu_xDy_y(WO_4)_3$ phosphor samples. The co-doping of $Eu^{3+}$ and $Dy^{3+}$ is more conducive to energy level transitions and improves its luminescence performance. Specifically, after the introduction of $Dy^{3+}$ ions, the charge transfer bands generated by the interaction between the host and $Eu^{3+}/Dy^{3+}$ ions partially overlap. With the increase of $Eu^{3+}$ ion doping concentration, the interaction between the two transfer bands is enhanced, resulting in a red shift in the UV–visible diffuse reflection absorption edge of the sample. Therefore, the emission color gradually changes from yellow through orange to red. This color transformation is likely due to the substitution of host ions, which alters the intensity of the crystal field surrounding the emission center. Overall, these findings offer valuable insights into the optical properties of doped phosphor materials, which could be beneficial for applications such as display screens, lighting, and sensing devices.

The variation UC emission spectra of the $NaSrGd_{0.7}Eu_{0.25}Dy_{0.05}(WO_4)_3$ over the temperature from 233 to 393 K is summarized in Fig. 6a–d. Obviously, the position and shape of each emission band in fluorescence spectrum are unchanged with the increasing of temperature from 233 to 393 K, while the emission intensity decreased caused by the thermal quenching phenomenon [33–35]. The decreased of the luminous intensity is also estimated with different temperature, as summarized in Fig. 6d. The luminous intensity decreases slightly with the increase of temperature from 100% at 233 K to 77.21% at 393 K under 393 nm excitation. Under the excitation of blue light at 464 nm, the emission intensity value decayed to 77.79% in the temperature region from 233 to 393 K. Especially for the region of 273–373 K, the luminescence intensity decayed is lower than 15% indicative of excellent thermal stability, which could meet the application requirements of LED phosphor working at harsh temperature.

The color coordinates of the $NaSrGd_{(-x-0.05)}Eu_xDy_{0.05}(WO_4)_3$($x=0.05$, 0.10, 0.15, 0.20, 0.25, 0.30, 0.35, 0.40) phosphors are investigated by calculated from the detected UC emission spectra. Figure 7a presents the Commission International de I'Eclairage (CIE) coordinate diagrams of $NaSrGd_{(1-x-0.05)}Eu_xDy_{0.05}(WO_4)_3$

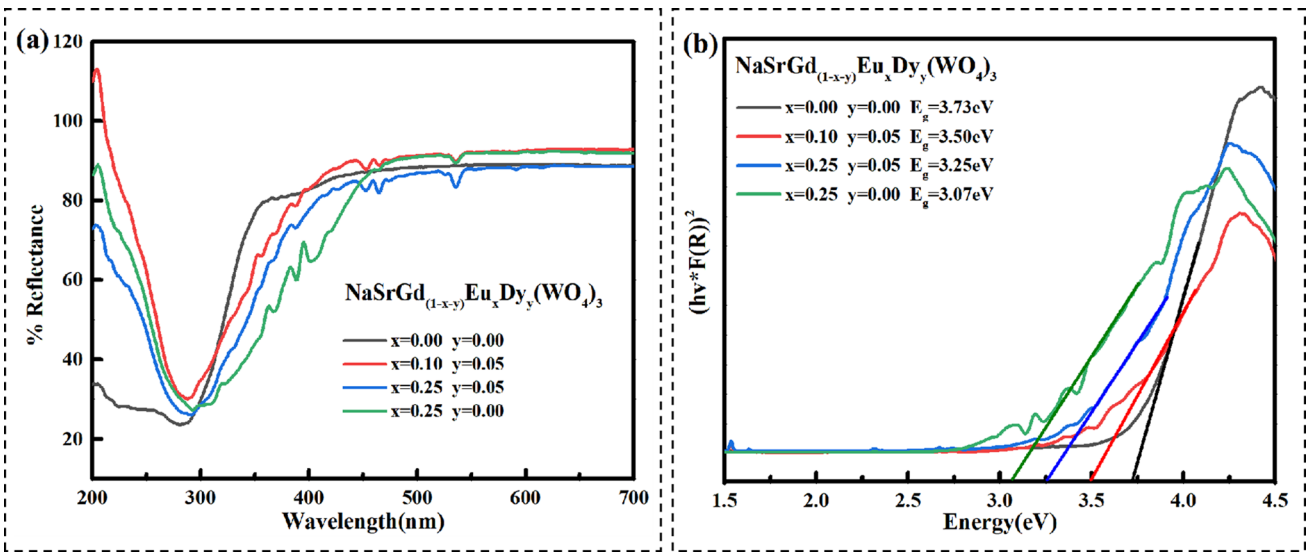


**Fig. 5** **a** UV-IR Diffuse Reflectance Spectra of the $NaSrGd_{(1-x-y)}Eu_xDy_y(WO_4)_3$phosphors; **b** Optical band gap diagram of the $NaSrGd_{(1-x-y)}Eu_xDy_y(WO_4)_3$ samples

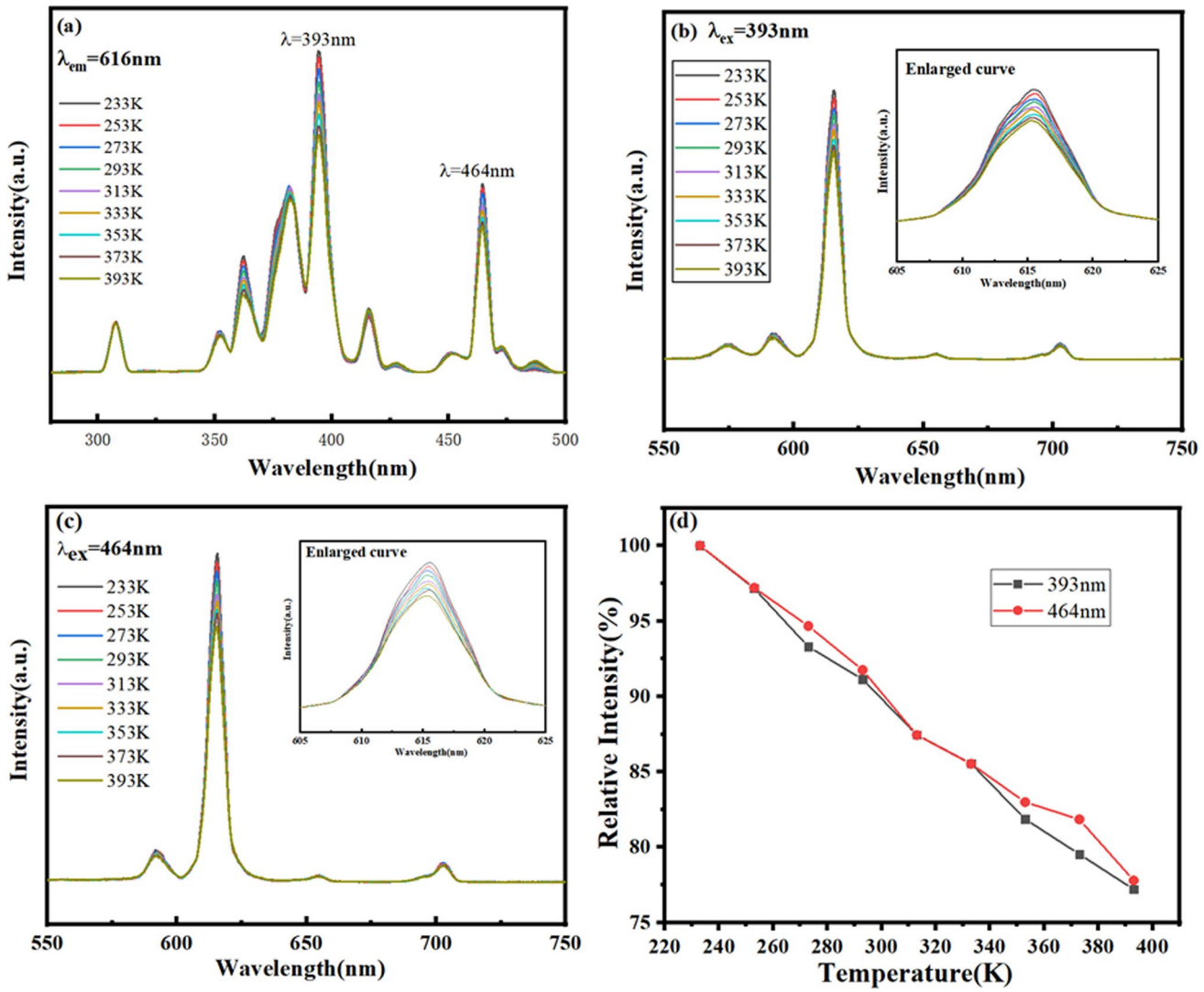


**Fig. 6** **a** Excitation spectra of $NaSrGd_{0.7}Eu_{0.25}Dy_{0.05}(WO_4)_3$ phosphor at variable temperature conversion ($\lambda_{em}=616$ nm); **b** Temperature varying conversion emission spectra of $NaSrGd_{0.7}Eu_{0.25}Dy_{0.05}(WO_4)_3$ phosphor ($\lambda_{ex}=393$ nm); **c** Temperature varying conversion emission spectra of $NaSrGd_{0.7}Eu_{0.25}Dy_{0.05}(WO_4)_3$ phosphor ($\lambda_{ex}=464$ nm); **d** Percentage diagram of peak emission light of $NaSrGd_{0.7}Eu_{0.25}Dy_{0.05}(WO_4)_3$ phosphor at different temperatures ($\lambda_{ex}=393$ nm, $\lambda_{ex}=464$ nm)

phosphors. The CIE coordinates for all prepared samples are located in the red region. The color purity for various $Eu^{3+}$ concentrations can be calculated by the numerical calculation of the color coordinates, as shown in Table 1. When the doping concentration of $Eu^{3+}$ ions is 25%, the color purity of the samples reaches more than 90%, which has great potential for technical application in the LED field. The relative brightness and color change diagram of the $NaSrGd_{(1-x-0.05)}\ Eu_xDy_{0.05}(WO_4)_3$ phosphor is displayed in Fig. 7b. With increasing of $Eu^{3+}$ ion doping concentration, the color of all the samples gradually changes from yellow to orange, and then to red. This feature makes this series of red phosphors can be used in white LED applications.

Figure 7c is a color-changing application device effect diagram prepared by $NaSrGd_{(1-x-0.05)}\ Eu_xDy_{0.05}(WO_4)_3$ phosphor samples. Clearly, the phosphor is white under visible light. After being excited by 365 nm UV light, the phosphor generally emits red light, which is the first-level anticounterfeiting achieved by ultraviolet excitation. In addition, different component phosphors show color gradient through ultraviolet excitation, generally from yellow to orange to red, which can be regarded as the second-level optical anticounterfeiting. More importantly, the color brightness is also significantly different as the composition changes, which can be regarded as the third-level optical anticounterfeiting. Combined with the above-mentioned three-level changes, the prepared color-changing device achieves a high level of optical safety with

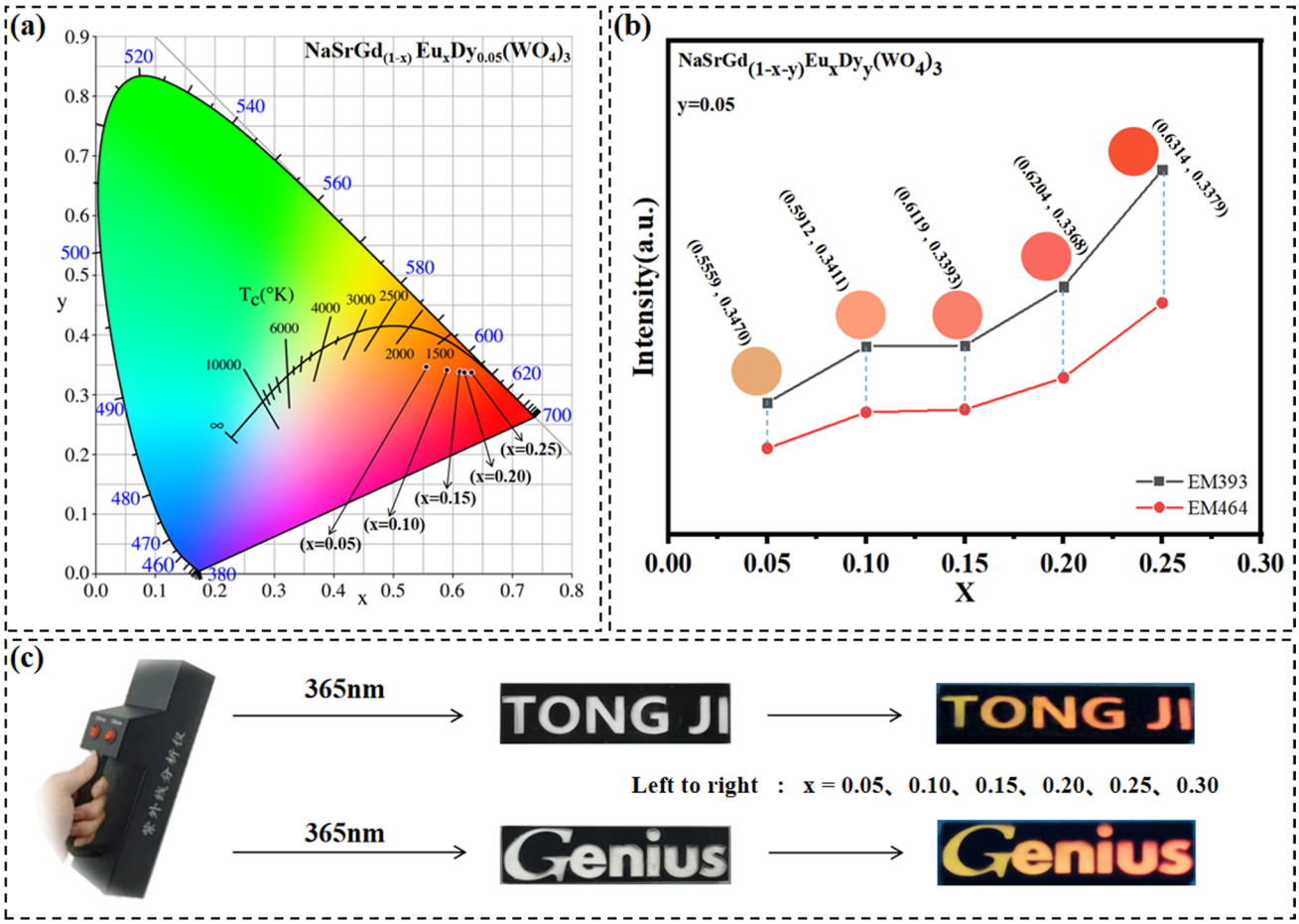


**Fig. 7** **a** CIE color coordinates of $NaSrGd_{(1-x)}Eu_xDy_{0.05}(WO_4)_3$ phosphor series samples; **b** Samples relative brightness and color change diagram; **c** Sample discoloration application example diagram (letters from left to right: $x = 0.05$, 0.10, 0.15, 0.20, 0.25, 0.25, 0.30)

**Table 1** The Coloration parameters of $NaSrGd_{(1-x-0.05)}Eu_xDy_{0.05}(WO_4)_3$ phosphor ($\lambda_{ex} = 393$ nm)

| $Eu^{3+}$ concentration $x$ (/mol) | Chromatic coordinate | Primary wavelength coordinate | Dominant wavelength(nm) | Color purity (%) |
|---|---|---|---|---|
| 0.05 | (0.5559, 0.3470) | (0.6470, 0.3526) | 604.692 | 70.96 |
| 0.10 | (0.5912, 0.3411) | (0.6566, 0.3431) | 607.271 | 79.77 |
| 0.15 | (0.6119, 0.3393) | (0.6594, 0.3403) | 608.069 | 85.43 |
| 0.20 | (0.6204, 0.3368) | (0.6624, 0.3373) | 608.973 | 87.23 |
| 0.25 | (0.6314, 0.3379) | (0.6614, 0.3384) | 608.657 | 90.86 |
| 0.30 | (0.6329, 0.3374) | (0.6619, 0.3378) | 608.827 | 91.16 |
| 0.35 | (0.6336, 0.3357) | (0.6638, 0.3359) | 609.399 | 90.86 |
| 0.4 | (0.6388, 0.3371) | (0.6624, 0.3374) | 608.948 | 92.84 |

mixed application objects, such as trademarks, banknotes or luxury goods, which have potential application in optical anti-counterfeiting [36].

## 4 Conclusions

$NaSrGd_{(1-x-y)}Eu_xDy_y(WO_4)_3$ powder red luminescent materials were synthesized by high-temperature solid-state reaction method. The samples are tetragonal scheelite structure. The effects of sintering temperature, doping concentration of $Eu^{3+}$ and $Dy^{3+}$ in $NaSrGd(WO_4)_3$ matrix, calcination temperature and working temperature on the microstructure and luminescence properties of the samples were investigated. The emission color of $NaSrGd(WO_4)_3:Dy^{3+}$ phosphor could be tunned via changing concentrations of $Eu^{3+}$ ion. In addition, the phosphors exhibit narrow red-light emission at 610 nm caused by the electric dipole transition $^5D_0 \rightarrow {}^7F_2$ of $Eu^{3+}$. Especially, the phosphor exhibits superior thermal stability, its emission intensity of optimum sample remained ± 15% over the temperature range from 233 to 393 K. The Commission International de I'Eclairage (CIE) chromaticity coordinates of $x = 0.4$ are (0.6388, 0.3371) with a high color purity (92.84%). More importantly, prepared color-changing device of phosphors achieves a high level of optical safety. has a bright future in the development of advanced light-emitting technologies and optical anti-counterfeiting.

**Acknowledgements** This work was supported by the National Natural Science Foundation of China (Grant No. 51572195).

**Author contributions** Hong Liu: methodology, supervision, writing-original draft preparation; Huihua Ye: methodology; RH: supervision; WL: methodology; JL: validation; ST: investigation, visualization; XW: writing-review and editing, funding, supervision; YL: supervision; XY: supervision.

**Data availability** The raw data required to reproduce these findings are available at authors and can be shared upon request.

## Declarations

**Conflict of interest** The authors declare that they have no conflicts to declare.

## References

1. Z. Xia, Q. Liu, Progress in discovery and structural design of color conversion phosphors for LEDs. Prog. Mater. Sci. **84**, 59–117 (2016)
2. N.C. George, K.A. Denault, R. Seshadri, Phosphors for solid-state white lighting. Annu. Rev. Mater. Sci. **43**(1), 481–501 (2013)
3. F.K. Yam, Z. Hassan, Innovative advances in LED technology. Microelectron. J. **36**(2), 129–137 (2004)
4. P. Falcaro, S. Furukawa, Doping light emitters into metal-organic frameworks. Angew. Chem. Int. Edit. **34**, 8431–8433 (2012)
5. K. Zhang, H.Z. Liu, W.B. Hu, Advances in the study of phosphor for white LEDs. J. Mater. Rep. **9**, 50–53 (2005)
6. S. Supriya, Highly tunable multifunctional rare earth based $Bi_{0.5-x}Ce_xNa_{0.5}TiO_3$ perovskites via site selective doping engineering. Mater. Chem. Phys. **287**, 126233 (2022)
7. Q. Zhang, X. Wang, X. Ding, Y. Wang, A potential red-emitting phosphor $BaZrGe_3O_9:Eu^{3+}$ for w-LED and FED applications: synthesis, structure, and luminescence properties. Inorg. Chem. **56**, 6990–6998 (2017)
8. L. Tang, L. Zhou, A. Liu, X. Yan, K. Zhong, X. Liu, X. Gao, J. Li, A new cascade reaction-based colorimetric and fluorescence "turn on" dual-function probe for cyanide and hydrazine detection. Dyes Pigm. **186**, 109034 (2021)
9. J. Zhong, Y. Peng, D. Chen, M. Liu, X. Li, Y. Zhu, Z. Ji, Highly efficient rare-earth free deep red emitting phosphor $La_2Li_{1-y}Sb_{1-x}O_6:xMn^{4+}, yMg^{2+}$: application in high-power warm w-LEDs. J. Mater. Chem. C. **6**(48), 13305–13315 (2018)
10. F. Zhang, W. Zhang, Z. Zhang, Y. Huang, Y. Tao, Luminescent characteristics and energy transfer of a red-emitting $YVO_4:Sm^{3+}$, $Eu^{3+}$ phosphor. J. Lumin. **152**, 160–164 (2014)
11. G. Li, Y. Wei, Z. Li, G. Xu, Synthesis and photoluminescence of $Eu^{3+}$ doped $CaGd_2(WO_4)_4$ novel red phosphors for white LEDs applications. Opt. Mater. **66**, 253–260 (2017)
12. P. Pust, V. Weiler, C. Hecht, A. Tücks, A.S. Wochnik, A.-K. Henß, D. Wiechert, C. Scheu, P.J. Schmidt, W. Schnick, Narrow-band red-emitting $Sr[LiAl_3N_4]:Eu^{2+}$ as a next-generation LED-phosphor material. Nat. Mater. **13**, 891 (2014)
13. D. Kang, H.S. Yoo, S.H. Jung, H. Kim, D.Y. Jeon, Synthesis and photoluminescence properties of a novel red-emitting $Na_2Y_2Ti_3O_{10}$: $Eu^{3+}$, $Sm^{3+}$ phosphor for whitelight-emitting diodes. J. Phys. Chem. C **115**, 24334–24340 (2011)
14. Y. Zhang, X. Li, K. Li, H. Lian, M. Shang, J. Lin, Crystal-site engineering control for the reduction of $Eu^{3+}$ to $Eu^{2+}$ in $CaYAlO_4$: structure refinement and tunable emission properties. ACS Appl. Mater. Interfaces **7**, 2715–2725 (2015)
15. J. Zhong, W. Zhao, E. Song, Y. Deng, Luminescence properties and dynamical processes of energy transfer in $BiPO_4:Tb^{3+}$, $Eu^{3+}$ phosphor. J. Lumin. **154**, 204–210 (2014)
16. X. Bai, Y. Cun, Z. Xu, Y. Zi, A.A. Haider, A. Ullah, I. Khan, J. Qiu, Z. Song, Z. Yang, Multiple anti-counterfeiting and optical storage of reversible dual-mode luminescence modification in photochromic $CaWO_4$: $Yb^{3+}$, $Er^{3+}$, $Bi^{3+}$ phosphor. Chem. Eng. J. **429**, 132333 (2022)
17. W. Zhang, J. Long, A. Fan, J. Li, Effect of replacement of Ca by Ln (Ln5Y, Gd) on the structural and luminescence properties of $CaWO_4:Eu^{3+}$ red phosphors prepared via co-precipitation. Mater. Res. Bull. **47**, 3479–3483 (2012)
18. V. Reshmi, P. Rao, M. Thomas, S. Mahesh, T.L. Francis, Enhanced $Eu^{3+}$ red luminescence in scheelite based oxides, $CaLaSbWO_8$. ECS J. Solid State Sci. Technol. **2**, R44–R48 (2013)
19. S. Bai, Y. Liu, G. Tan, H. Ren, D. Liu, K. Wang, R. Wang, Y. Zhu, S. Ye, Novel multiwavelength effectively excited $ZnWO_4$-$WO_3:Eu^{3+}$ multiphase red phosphor for white light-emitting diodes. J. Alloy. Compd. **807**, 151668 (2019)
20. S. Supriya, Synthesis mechanisms and effects of $BaTiO_3$ doping on the optical properties of $Bi_{0.5}Na_{0.5}TiO_3$ lead-free ceramics. J. Solid State Chem. **308**, 122940 (2022)
21. S. Supriya, A critical review on crystal structure mechanisms, microstructural and electrical performances of

$Bi_{0.5}Na_{0/5}TiO_3$-$SrTiO_3$ perovskites. J. Electroceram.Electroceram. **49**, 94–108 (2022)
22. R. Krishnan, J. Thirumalai, I. Banu, A. Peter, Rugby-ball-shaped $Na_{0.5}La_{0.5}MoO_4$:$Eu^{3+}$ 3D architectures: synthesis, characterization, and their luminescence behavior. J. Nanostruct. Chem. **3**, 14 (2013)
23. S. Supriya, Effect of sintering temperature and micro structural analysis on sol–gel derived silver bismuth titanate ceramics. Mater. Res. Bull. **96**, 290–295 (2017)
24. S. Supriya, Effect of doping and enhanced microstructures of bismuth titanates as aurivillius perovskites. Micron **162**, 103344 (2022)
25. C.M. Kuo, P.C. Kuo, W.C. Hsu, C.T. Li, A.C. Sun, Effects of W and Ti on the grain size and coercivity of $Fe_{50}Pt_{50}$ thin films. J. Magn. Magn. Mater. **209**, 100–102 (2000)
26. C. Zollfrank, S. Gruber, M. Batentschuk, A. Osvet, F. Goetz-Neunhoeffer, S. Dittrich, J. Grabow, H.-D. Kurland, F.A. Müller, Synthesis of Eu-doped $SrAl_2O_4$ nanophosphors by $CO_2$ laser vaporization. Acta Mater. **61**, 7133–7141 (2013)
27. P. Dorenbos, Energy of the $Eu^{2+}$ 5d state relative to the conduction band in compounds. J. Lumin. **128**, 578–582 (2008)
28. Y. Kim, Z. Hu, I. Avdeev, A. Singh, A. Singh, V. Chandrasekaran, M. Nestoklon, S. Goupalov, J. Hollingsworth, H. Htoon, Interplay of bright triplet and dark excitons revealed by magneto-photoluminescence of individual PbS/CdS quantum dots. Small **17**, 2006977 (2021)
29. G. Lakshminarayana, A. Wagh, S. Kamath, A. Dahshan, H. Hegazy, M. Marzec, I. Kityk, D. Lee, J. Yoon, T. Park, $Eu^{3+}$-doped fluoro-telluroborate glasses as red-emitting components for W-LEDs application. Opt. Mater. **99**, 109555 (2020)
30. D. Lapaev, V. Nikiforov, V. Lobkov, A. Knyazev, A. Krupin, Y. Galyametdinov, New insights into UV laser irradiation effect on luminescent behavior of vitrified films based on mesogenic lanthanide(III) beta-diketonate complexes. J. Photoch. Photobio. **382**, 111962 (2019)
31. X. Liu, R. Pang, Q. Li, J. Lin, Host-sensitized luminescence of Dy3+, Pr3+, Tb3+ in polycrystalline $CaIn_2O_4$ for field emission displays. Int. J. Quantum Chem. **180**(4), 1421–1430 (2007)
32. Z. Zhang, A. Song, X. Shen, Q. Lian, X. Zheng, A novel white emission in $Ba_{10}F_2(PO_4)$(6:)$Dy^{3+}$ single-phase full-color phosphor. Mater. Chem. Phys. **151**, 151345 (2015)
33. Y. Huang, L. Zhou, L. Yang, Z. Tang, Self-assembled 3D flower-like $NaY(MoO_4)_2$:$Eu^{3+}$ microarchitectures: hydrothermal synthesis, formation mechanism and luminescence properties. Opt. Mater. **33**(6), 777–782 (2011)
34. W. Xie, H. Huang, J. Li, Z. Wang, C. Tian, M. Xie, C. Zou, G. Sun, Controlling the energy transfer via multi luminescent centers to achieve white/tunable light in a single-phased $Sc_2O_3$:$Bi^{3+}$, $Eu^{3+}$ phosphor. Ceram. Int. **S02**(72), 88–112 (2018)
35. H. Yamamoto, S. Seki, J.P. Jeser, T. Ishiba, Thermal quenching of luminescence in a disordered compound: $EuNa_2Mg_2(VO_4)_3$. J. Electrochem. Soc. **127**(3), 694–701 (1980)
36. B.H. Min, K.Y. Jung, Luminescence improvement of (Ti, Si)$O_2$: $Eu^{3+}$/$Li^+$ spherical particles for anti-counterfeiting application. Mater. Chem. Phys. **267**, 124612 (2021)